Electronic, magnetic and elastic properties of ε−phases Fe3X(X=B, C, N) from density-functional theory calculations

ARTICLE *in* JOURNAL OF MAGNETISM AND MAGNETIC MATERIALS · JULY 2012

Impact Factor: 1.97 · DOI: 10.1016/j.jmmm.2012.02.114

6 AUTHORS, INCLUDING:

Zhiqing Lv
Yan Shan University
31 PUBLICATIONS **240** CITATIONS
SEE PROFILE

Wan-tang Fu
Yan Shan University
55 PUBLICATIONS **363** CITATIONS
SEE PROFILE

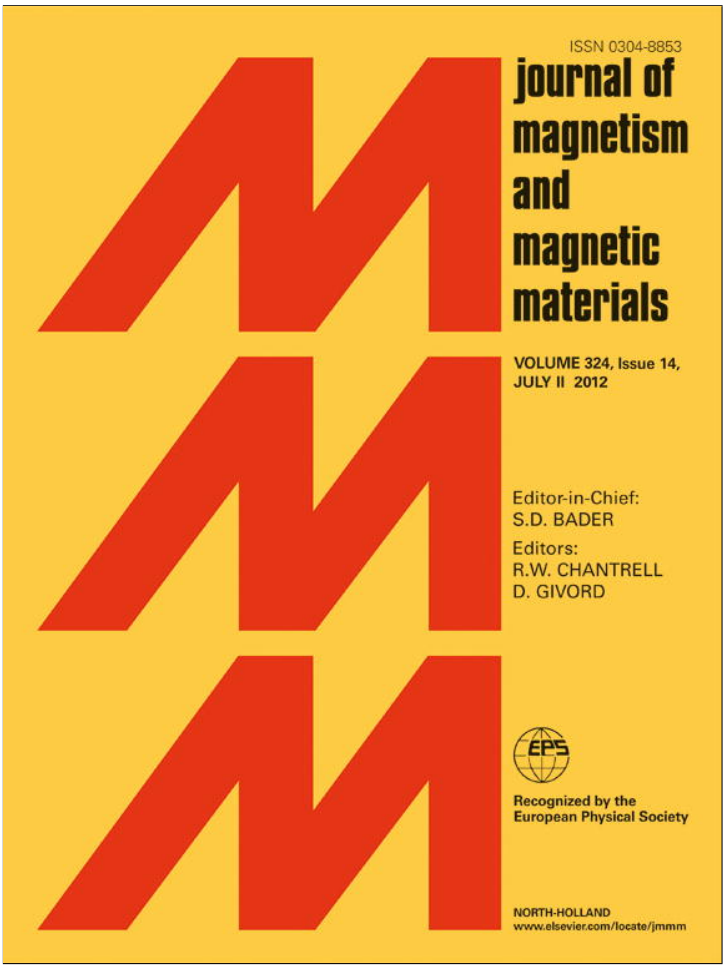

Journal of Magnetism and Magnetic Materials 324 (2012) 2271–2276

Contents lists available at SciVerse ScienceDirect

Journal of Magnetism and Magnetic Materials

journal homepage: www.elsevier.com/locate/jmmm

Electronic, magnetic and elastic properties of ε-phases Fe_3X(X=B, C, N) from density-functional theory calculations

W.H. Zhang [a], Z.Q. Lv [a,b,*], Z.P. Shi [b], S.H. Sun [c], Z.H. Wang [a,b], W.T. Fu [a,*]

[a] State Key Laboratory of Metastable Material Science and Technology, Yanshan University, Qinhuangdao 066004, China
[b] College of Mechanical Engineering, Yanshan University, Qinhuangdao 066004, China
[c] College of Science, Yanshan University, Qinhuangdao 066004, China

ARTICLE INFO

Article history:
Received 15 January 2012
Received in revised form
20 February 2012
Available online 3 March 2012

Keywords:
Metastable phase
Magnetic property
First principle
Crystal structure

ABSTRACT

First principles calculations have been performed for ε-phases Fe_3X(X=B/C/N) with hexagonal close-packed Fe sublattices. The calculated equilibrium structural parameters of ε-Fe_3C and ε-Fe_3N are in agreement with experimental results. The crystal structure of the ε-Fe_3B is predicted. In the view of the formation energy, the phase stabilities grow up from ε-Fe_3B, θ-Fe_3N, ε-Fe_3C, θ-Fe_3C, θ-Fe_3B to ε-Fe_3N. The bonding nature in ε-Fe_3X (X=B/C/N) is described as a complex mixture of covalent, ionic and metallic characters. The average magnetic moments (Ms) of the ε-Fe_3B, ε-Fe_3C and ε-Fe_3N are 1.53, 1.61 and 1.66 μ_B/atom, respectively. The Ms of Fe are 2.17, 2.23 and 2.25 μ_B in ε-Fe_3B, ε-Fe_3C and ε-Fe_3N, respectively. The Ms of B/C/N are $-0.39/-0.26/-0.08$ μ_B.The Debye temperatures of ε-Fe_3X (X=B/C/N) are predicted as 427, 565 and 555 K.

1. Introduction

Iron carbides, nitrides and borides play an important role in iron alloys and steels, which usually exist in steels with orthorhombic and hexagonal structure [1–5]. The θ-Fe_3C with orthorhombic structure is the one of key phases in the white cast iron and steels. The ε iron carbides (ε-$Fe_{2-3}C$) precipitate during the tempering processes of martensite[5–8]. Nitrogen and Boron have been introduced into steels to improve their properties, which mainly forms solid solution and compounds with Fe (Fe_4N/$Fe_{2-3}N$/$Fe_{2-3}B$ etc.) [2,3]. In some cases, Fe_3B and Fe_3N are also the important phases in some magnetic materials [3,4]. Knowledge about the stability and properties of Fe_3X (X=B/C/N) is useful for understanding the evolution rule of alloying compounds in the processes and treatments of the steels. So many experimental and theoretical studies have been carried out on the crystal structures and properties of these phases [7–15]. Fang and co-workers [7,8] studied the stability and structures of ε-phases of iron nitrides and iron carbides using the density functional theory within the projector-augmented wave method (PAW), and the formation energies of ε-$Fe_{2-3}C$ and ε-$Fe_{2-3}N$ were calculated, but the ε-borides with hexagonal structure was not referred to. Jang and co-workers [9] calculated the stability of ε-carbide in transformation-induced plasticity (TRIP) aided steels by the use of the full-potential linearized augmented-plane-waves method (PLAPW), and confirmed ε-carbide unstably in the TRIP steels. Rainer and co-workers [10] investigated the single-crystal growth and electronic structure of ε-Fe_3N_{1+x}, while Liapin et al. [11] studied the structural properties of the ε-Fe_3N_{1+x} phases further. Shang and co-workers [12] studied the structural behavior of the ε-nitrides by means of the first principles calculations, and indicated the crystal characters of them. The carbides and borides with the same structure were not investigated in depth by them. The structures of ε-Fe_3N phases were confirmed by them. Kong and Li [13] investigated the cohesive energy, local magnetic properties and Curie temperature of Fe_3B using the self-consistent linear muffin-tin orbitals (LMTO) method, and the magnetic properties and Curie temperature of θ-Fe_3B were obtained. Medvedeva and co-workers [14] simulated the structural, electronic and magnetic properties of θ-$Fe_3C_{1-x}B_x$, and gave the change of magnetic properties of θ-$Fe_3C_{1-x}B_x$ with different contents of C and B. We calculated the mechanical, electronic and magnetic properties of ε-Fe_3C and θ-Fe_3C using the pseudo-potential plane–wave within the density functional theory, and indicated the stability relationship between ε-Fe_3C and θ-Fe_3C [15]. Recently, we performed the first-principles calculations on cementite-type Fe_3X (X=B/C/N) with orthorhombic structure and showed the electronic and magnetic properties of them, and addressed the differences of them [16]. And the electronic and magnetic properties of alloyed cementite (Cr/Mn/Co/Ni) with orthorhombic structure were also investigated and addressed the differences of them [17,18]. However, the

* Corresponding authors at: Yanshan University, State Key Laboratory of Metastable Material Science and Technology, Qinhuangdao 066004, China.
Tel.: +86 335 8074036; fax: +86 335 805 7068.
E-mail addresses: zqlv@ysu.edu.cn (Z.Q. Lv), wtfu@ysu.edu.cn (W.T. Fu).

0304-8853/$ - see front matter © 2012 Published by Elsevier B.V.
doi:10.1016/j.jmmm.2012.02.114

electronic, magnetic and elastic properties of ε phases Fe_3X with hexagonal structure and the differences of them are not fully clear so far.

The present study aims to examine the magnetic and elastic properties of ε-Fe_3X (X=B/C/N) and to clarify the relationship between them using the first-principles method. The formation energies of ε-Fe_3X and θ-Fe_3X(X=B/C/N) are calculated and compared, and the structural properties of the ε-Fe_3B are predicted. We also predicted the elastic properties and Debye temperatures (θ_D) of ε-Fe_3X (X=B/C/N).

2. Crystal structure and calculation details

2.1. Structural models of ε-Fe_3X

The ε-Fe_3X (X=B/C/N) crystallizes in the hexagonal space group $P6_322$ (S.G. no. 182) with two formula units ($Z=2$) per unit cell, where six iron atoms and two nonmetal atoms in the interstices [19,20]. A three-dimensional drawing of the unit cell is shown in Fig. 1.

2.2. Stability of ε-Fe_3X

The formation enthalpy (ΔH) of Fe_3X (X=B/C/N) from the elements (α-Fe, graphite, alpha-boron and molecular N_2) can be described as:

$$\Delta H = E(Fe_3X) - 3E(Fe) - E(X) \quad (1)$$

At $T=0$ K and $p=0$ Pa, the formation enthalpy equals the calculated formation energy (ΔE), i.e. $\Delta H(Fe_3X)=\Delta E(Fe_3X)$, when the zero-vibration contribution is ignored [7,8,15]. The formation enthalpy/energy defined in this way can be used to measure the thermodynamic stability of Fe_3X with respect to the α-Fe, graphite, alpha-boron and molecular N_2.

The mechanical stability of a crystal implies that the strain energies are positive. The mechanical stability of the crystal is described with elastic constants C_{ij} depending on the crystal structure. For the hexagonal crystal structures such as ε-Fe_3C, ε-Fe_3N or ε-Fe_3B, there are five different symmetry elements (C_{11}, C_{33}, C_{44}, C_{12}, C_{13}). The stability criteria for a hexagonal crystal are [15,21]:

$$C_{11}>0, C_{11}-C_{12}>0, C_{44}>0, (C_{11}+C_{12})C_{33}-2C_{13}^2>0 \quad (2)$$

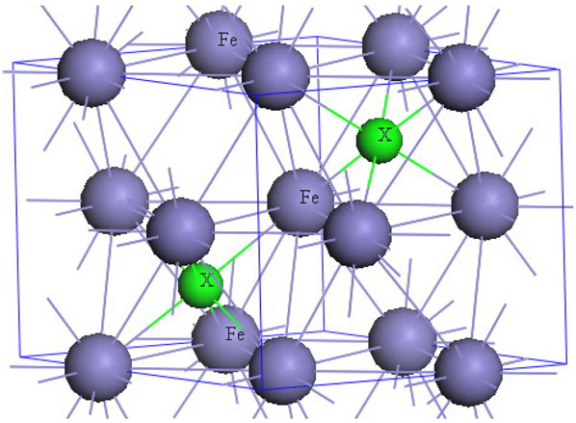

Fig. 1. Crystal structure of ε-Fe_3X (X=B/C/N), showing the hexagonal space lattice .

2.3. Method of calculations

All calculations were performed based on the pseudo-potential plane–wave within the density functional theory [22,23] using the Cambridge Serial Total Energy Package (CASTEP) [24]. The exchange-correlation potential was evaluated using the Perdew-Burke-Eruzerhof functional [25] within the generalized gradient approximation (PBE-GGA) [26].The interactions between the core and valence electrons were described by ultra-soft pseudo-potentials [27], and the Kohn-Sham one-electron states were expanded in a plane wave basis set up to 300 eV. The energy calculations in the first irreducible Brillouin zone were conducted by using $6\times6\times6$ k-point grid of Monkhorst-Pack scheme [28]. The convergence criteria for structure optimization and energy calculation were set to fine quality with the tolerance for the stress concentration factor (SCF), energy, maximum force and maximum displacement of 10^{-6} eV/atom, 10^{-5} eV/atom, 0.03 eV/Å and 0.001 Å, respectively. Because of its large effect on magnetic systems, spin polarization was included in the calculations to correctly account for its magnetic properties. After getting equilibrium geometry, the elastic constants were obtained using the stress-strain method [29,30].

3. Results and discussions

3.1. Structure optimization

The ground state properties of the ε-Fe_3X (X=B/C/N) are investigated from their total energy, which is calculated as a function of volume. According to the Murnaghan equation of state [31], the equilibrium lattice constants and atomic positions can be obtained (see Table 1). It can be found that the calculated values of the lattice constants match fairly well with the experimental ones for ε-Fe_3C [19] and ε-Fe_3N [20]. The deviations between the experimental and theoretical values of cell volume are smaller than 1% for ε-Fe_3N and ε-Fe_3C, respectively. Using the same method, the crystal structure of the ε-Fe_3B is predicted (shown

Table 1
Experimental (values within brackets) and calculated lattice constants a_0, b_0, c_0 (Å), v_0 (Å^3), ρ(g/cm^3), atom sites of ε-Fe_3B, ε-Fe_3C and ε-Fe_3N.

	ε-Fe_3B	ε-Fe_3C	ε-Fe_3N
$a=b$	4.73088	4.67806(4.767[A],4.6572[C])	4.69140(4.6982[B],4.6559[C])
c	4.44060	4.34961(4.354[A],4.3143[C])	4.34551(4.3789[B],4.3180[C])
a/c	1.065	1.076 (1.095[A], 1.079[C])	1.08 (1.073[B],1.078[C])
Fe	0.30748,0,0	0.32504,0,0	0.32899,0,0
X	1/3,2/3,0.25	1/3,2/3,0.25	1/3,2/3,0.25
V	86.07	82.44	82.83
ρ	6.88	7.23	7.28

[A] Reference [17].
[B] Reference [18].
[C] Reference [8].

in Table 1). Considering the similarity of GGA values with experimental data, subsequent calculations were carried out using GGA. The energetic and mechanical stabilities are addressed in section 3.2. Details of the electronic properties and magnetic properties of ε-Fe_3X are analyzed in section 3.3. Elastic properties and Debye temperatures of ε-Fe_3X (X=B/C/N) are calculated in section 3.4 and section 3.5, respectively.

3.2. Stability of phases

The calculated formation enthalpies of ε-Fe_3X (X=B/C/N) are shown in Fig. 2. The formation enthalpies of θ-Fe_3X (X=B/C/N) were also calculated using the same method based on the cementite structure in the literature [16]. The formation energies are shown in Fig. 2. The relative stability relationships between ε- and θ-Fe_3X (X=C/N) are agreement with the result in the literature [8]. In the view of the formation energy, the phase stability grows up from ε-Fe_3B, θ-Fe_3N, ε-Fe_3C, θ-Fe_3C, θ-Fe_3B to ε-Fe_3N. The formation energies of ε-Fe_3N (-0.255 eV/f.u.) and θ-Fe_3B (-0.08 eV/f.u.) are negative, which indicates that the formation of ε-Fe_3N and θ-Fe_3B are easier than other phases in the steels or Fe-N/B alloys. The formation energy of ε-Fe_3N is close to the other calculation [8]. From the calculation results, the formation energies of ε-Fe_3B and θ-Fe_3N are positive and bigger than other phases in this calculation, which shows that ε-Fe_3B and θ-Fe_3N form more difficultly than ε-Fe_3X (X=C/N) and θ-Fe_3X (X=B/C).

The elastic constants of ε-Fe_3X (X=B/C/N) were calculated at their equilibrium lattice constants and optimized structure. The theoretical elastic constants are listed in Table 2. From the results, we can find ε-Fe_3X (X=B/C/N) are mechanically stable as their elastic constants satisfy with formula (2), respectively.

3.3. Electronic and magnetic properties of phases

In this part, the electronic structures of these ε-phases will be discussed and compared with each other. Fig. 3 depicts the calculated site- and spin-projected DOSs (density of states) for ε-Fe_3X (X=B/C/N). It can be seen that there are no energy gap near to the Fermi level. This shows a metallic nature of ε-Fe_3X (X=B/C/N). In addition, the energy gaps between the lowest valence band and the upper valence band are 0.5, 4.1 and 7.9 eV for ε-Fe_3B, ε-Fe_3C and ε-Fe_3N, respectively. This indicates that the chemical bonds of ε-Fe_3X (X=B/C/N) take on ionicity and the ionicity of Fe-X strengthens from Fe-B, Fe-C to Fe-N. The main reason for the ionicity of Fe-X is the difference in electronegativity between Fe and X. Fig. 4 shows the spin-projected Partial Densities of States (PDOSs) for ε-Fe_3X (X=B/C/N), respectively. From Fig. 4, it can be seen that Boron's 2s band lies in -7 and -10 eV, Carbon's 2s band ranges from -11 to -15 eV and Nitrogen's 2s band locates at -17.5 and -16 eV. The Fe's 4s band is affected by 2s band of X (B/C/N) atom, and their distributions accord with B/C/N atoms in ε-Fe_3X (X=B/C/N). From about -8 to -5 eV, there exists the hybridization of X 2p and Fe 3d. Near the Fermi level, the calculated DOS profiles of these phases are dominated by Fe's 3d band.

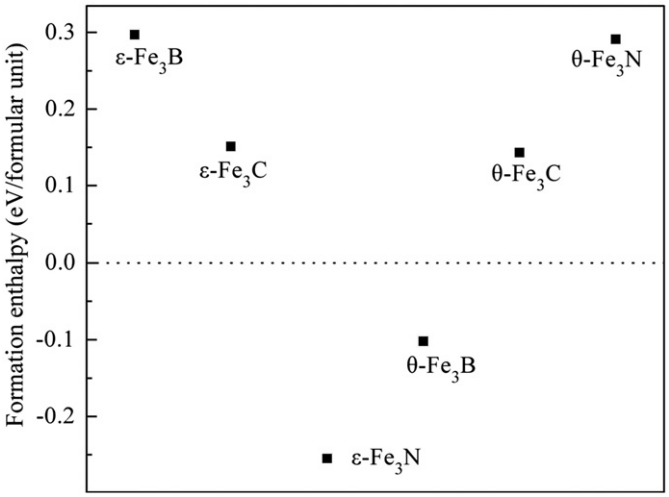

Fig. 2. The calculated formation enthalpies of the ε- and θ-Fe_3X (X=B/C/N).

Table 2
Calculated elastic constants of ε-Fe_3B, ε-Fe_3C and ε-Fe_3N (C_{ij} in GPa).

	C_{11}	C_{12}	C_{13}	C_{33}	C_{44}
ε-Fe_3B	219.5	131.7	80.2	143.1	72.3
ε-Fe_3C	307.9	139.7	127.6	320.6	118.5
ε-Fe_3N	276.0	94.5	120.6	325.3	109.1

In Fig. 5, the electron density distribution map of ε-Fe_3X is plotted in the way of the electron density difference map. The electron density difference was determined as $\Delta\rho=\{\rho_{crystal}-\sum\rho_{at}\}$, where $\rho_{crystal}$ and ρ_{at} are the valence electron densities for ε-Fe_3X (X=B/C/N) and the corresponding free atoms, respectively. It can be seen that the electron densities near Fe atom decrease and the electron densities of nonmetal (B/C/N) atoms increase. There exist the loss and gain of electrons between Fe atom and X atom along the Fe-X direction. The increment of valence electrons is concentrated on the X (X=B/C/N) atoms. In the interstitial regions, the increment of delocalized electrons is attributed to the metallic bonds. The calculated lengths of the Fe-B bonds are 1.9795 Å, and the corresponding overlapping population values are 0.29 in ε-Fe_3B. The calculated lengths of the Fe-C bonds are 1.9214 Å, and the corresponding overlapping population values are 0.30 in ε-Fe_3C. The lengths of the Fe-N bonds are 1.9126 Å, and the corresponding overlapping-population values are 0.25 in ε-Fe_3N. This indicates that the strong covalent bonding states exist in ε-Fe_3X (X=B/C/N). From the analyses of electronic structure, the bonding nature of ε-Fe_3X (X=B/C/N) may be described as a mixture of covalent-ionic, due to the d-resonance in the vicinity of the Fermi level, and be partly metallic characters. The lengths of Fe-Fe bonds in ε-Fe_3B, ε-Fe_3C and ε-Fe_3N are 2.6570∼2.8659 Å, 2.6482∼2.7437 Å and 2.6652∼2.7264 Å, respectively. There are no negative overlap population values of Fe-Fe bonds in ε-Fe_3X (X=B/C/N), which indicates no repulsion force among these atoms.

The spin components and the spin magnetic moments (Ms) of each atom in ε-Fe_3X (X=B/C/N) were calculated according to the Mulliken scheme. The values of atom Ms can be obtained from the deviation between the up spin occupied state and down spin occupied state, which are listed in Table 3. The magnetic moments of Fe are 2.17 μ_B, 2.23 μ_B and 2.25 μ_B in ε-Fe_3B, ε-Fe_3C and ε-Fe_3N, respectively. The Ms of B/C/N are $-0.39/-0.26/-0.08$ μ_B. The average magnetic moments of the ε-Fe_3B, ε-Fe_3C and ε-Fe_3N are 1.53, 1.61 and 1.66 μ_B/atom, respectively.

3.4. Elastic properties of phases

Table 2 includes the elastic constants C_{ij} of ε-Fe_3B, ε-Fe_3C and ε-Fe_3N. Once the elastic constants are determined, we would like to compare our results with experiments, or predict what an experiment would yield for the elastic constants. Up to date, no direct experimental elastic constants are available to be compared with our theoretical results. Future experimental measurements will provide a comparison for our calculated predictions. A problem arises when single crystal samples cannot be obtained.

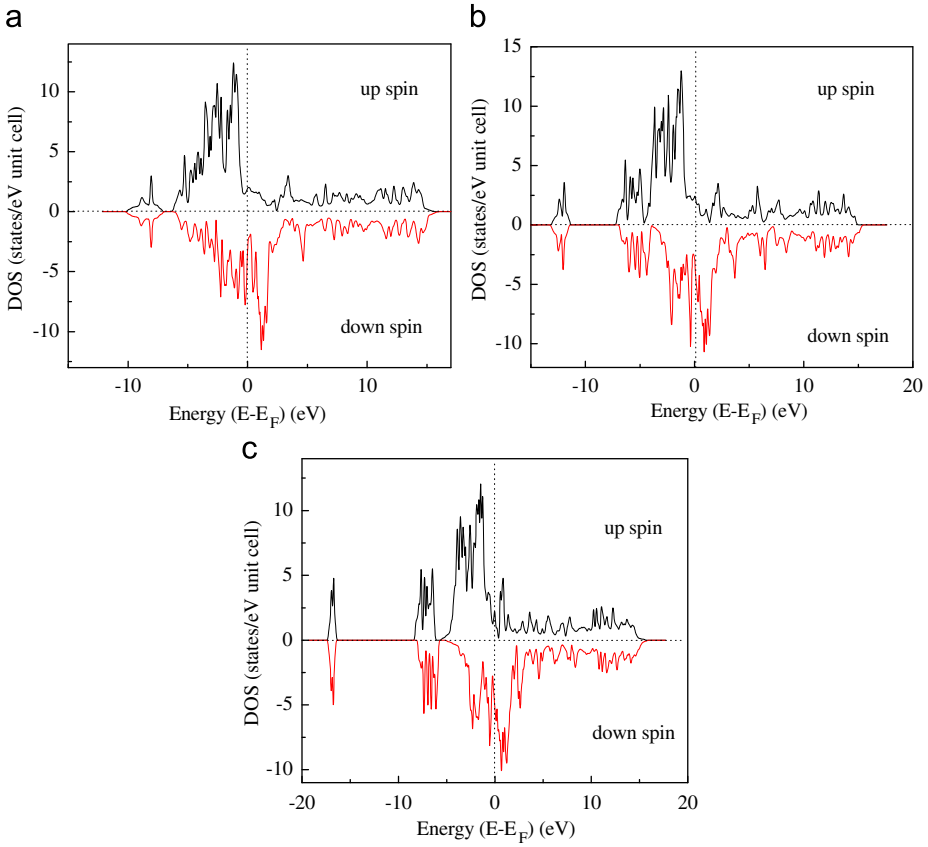

Fig. 3. Calculated spin-polarized total density of states of (a) ε-Fe_3B (b) ε-Fe_3C (c) ε-Fe_3N.

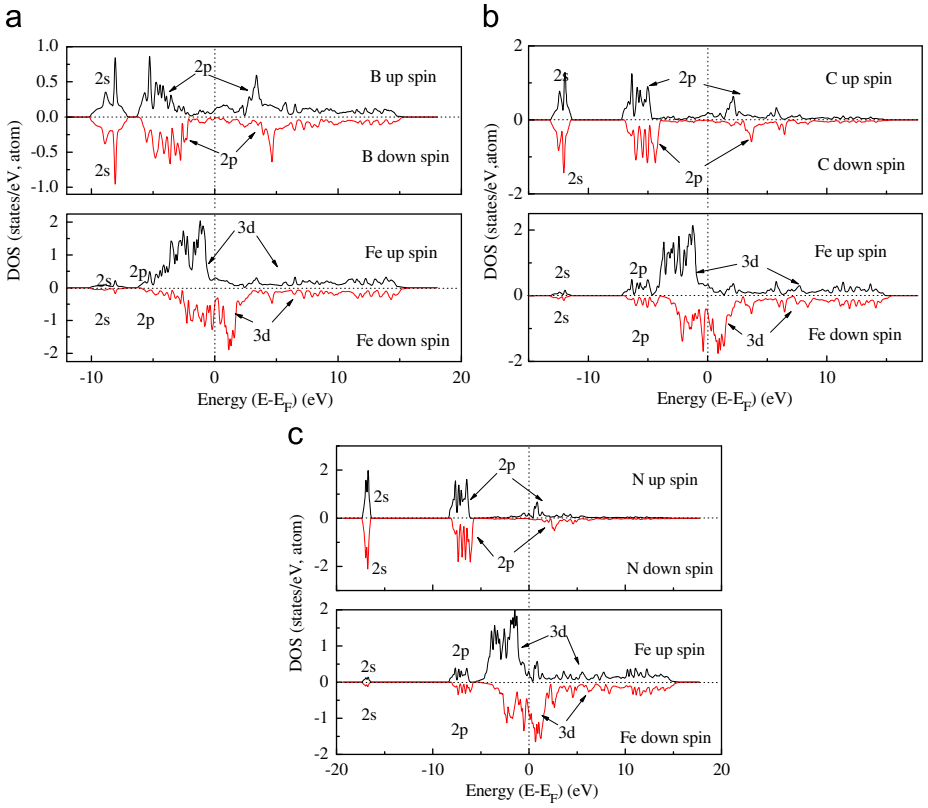

Fig. 4. Calculated spin-up and spin down partial density of states of (a) ε-Fe_3B (b) ε-Fe_3C (c) ε-Fe_3N.

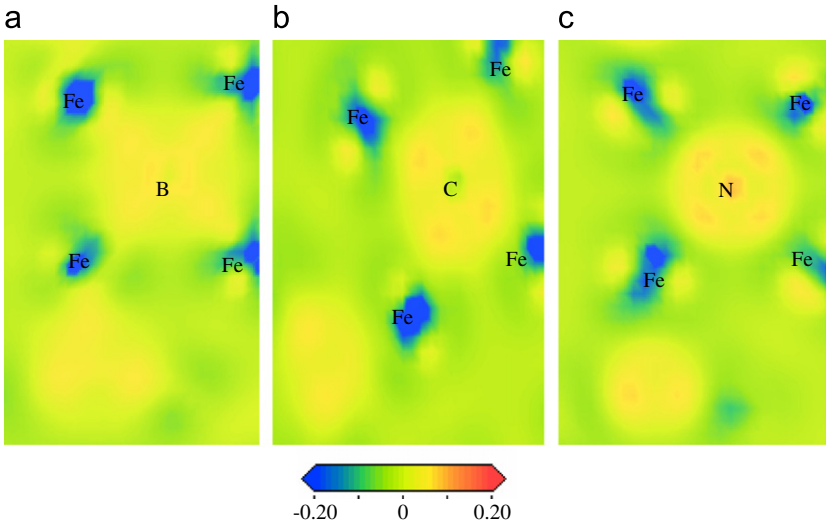

Fig. 5. Electron density difference map of the plane with Fe-X bonds of ε-Fe_3X (X=B/C/N) plotted from −0.2 (blue) to 0.2 (red) e $Å^{-3}$ (a) ε-Fe_3B (b) ε-Fe_3C (c) ε-Fe_3N. (For interpretation of the references to colour in this figure legend, the reader is referred to the web version of this article.)

Table 3
Calculated magnetic moments of each atom and ε-Fe_3B, ε-Fe_3C and ε-Fe_3N.

Species	Fe (μ_B/atom)	X (μ_B/atom)	Ms (μ_B/f.u.)
ε-Fe_3B	2.17	−0.39	6.12
ε-Fe_3C	2.23	−0.26	6.42
ε-Fe_3N	2.25	−0.08	6.64

Table 4
Calculated Voigt's bulk modulus (B_v), Reuss's bulk modulus (B_R), effective bulk modulus (B), Voigt's shear modulus (G_v), Reuss's shear modulus (G_R), effective shear modulus (G), Young's modulus (E in Gpa), and Poisson's ratio (v) for ε-Fe_3B, ε-Fe_3C and ε-Fe_3N.

	B_V	B_R	B	G_V	G_R	G	E	B/G	v
ε-Fe_3B	129.6	118.1	123.9	57.0	23.2	55.1	144.0	2.25	0.306
ε-Fe_3C	191.8	191.8	191.8	100.3	98.0	99.2	253.8	1.93	0.279
ε-Fe_3N	172.1	169.7	170.9	97.9	96.8	97.3	245.3	1.76	0.260

Then it is impossible to measure the individual elastic constants C_{ij}. Instead, the isotropic bulk modulus B and shear modulus G are determined [32]. These quantities cannot in general be calculated directly from the Cij, but we can use our values to place bounds on the isotropic moduli. Reuss found lower bounds for all lattices [33], while Voigt discovered upper bounds [34]. Hill [35] shown that the Voigt and Reuss averages were limits and suggested that the actual effective moduli could be approximated by the arithmetic mean of the two bounds. The formulas, for these bounds for hexagonal lattice can be found in literature [32]. We also calculated the Young's modulus (E) and Poisson's ratio (σ). These quantities are related to the bulk modulus B and the shear modulus G by the following equations [36]:

$$E = 9BG/(3B+G) \tag{3}$$

$$v = (3B-E)/6B \tag{4}$$

The calculated Voigt's bulk modulus (B_v), Reuss's bulk modulus (B_R), effective bulk modulus (B),Voigt's shear modulus (G_v), Reuss's shear modulus (G_R), effective shear modulus (G), Young's modulus (E), and Poisson's ratio (v) of ε-Fe_3B, ε-Fe_3C and ε-Fe_3N are given in Table 4.

The ratio of B to G gives us an estimation of the degree of ductility [37]. The ratios of ε-Fe_3X (X=B/C/N) are higher than the critical value 1.75, separating ductile and brittle behavior of a material. The bigger the ratio, the higher the ductility is. It can be seen that the three phases are not brittle materials. The bulk modulus of ε-Fe_3B is smallest in the three phases, and the ductility of ε-Fe_3B (2.25) is better than that of ε-Fe_3X (X=C/N).

Table 5
Calculated longitudinal, transverse, average sound velocity (v_l, v_t, v_m in m/s) and the Debye temperature (θ_D in K) from polycrystalline elastic modulus of ε-Fe_3B, ε- Fe_3C and ε-Fe_3N.

	v_l	v_t	v_m	θ_D
ε-Fe_3B	5356	2830	3164	427
ε-Fe_3C	6695	3704	4127	565
ε-Fe_3N	6426	3656	4064	555

3.5. Calculation of Debye temperature

Debye temperature is an important fundamental parameter closely related to many physical properties such as elastic constants, specific heat and melting temperature. One of the standard methods to calculate the Debye temperature (θ_D) is from elastic constants data, since θ_D may be estimated from the average sound velocity v_m by the following equation [38]:

$$\theta_D = \frac{h}{k_B}\left[\frac{3n}{4\pi V}\right]^{1/3} v_m \tag{5}$$

where h is Plank's constant, k_B is Boltzmann's constant, n is the number of atoms in cell and V is the cell volume. The average sound velocity in the polycrystalline material is given by [36]:

$$v_m = \left[\frac{1}{3}\left(\frac{2}{v_t^3}+\frac{1}{v_l^3}\right)\right]^{-1/3} \tag{6}$$

where v_l and v_t are the longitudinal and transverse sound velocity obtained using the shear modulus G and the bulk modulus B from Navier's equation [36]:

$$v_t = \left(\frac{3B+4G}{3\rho}\right)^{1/2} \text{ and } v_l = \left(\frac{G}{\rho}\right)^{1/2} \tag{7}$$

The calculated sound velocity and Debye temperature of ε-Fe_3X (X=B/C/N) are given in Table 5. The Debye temperatures (θ_D) of ε-Fe_3X (X=B/C/N) are 427 K, 565 K and 555 K, respectively.

Unfortunately, as far as we know, there are no data available related to these properties in the literature for ε-Fe_3X (X=B/C/N), therefore our calculated values can be considered as prediction of these properties for these compounds. Future experimental work will testify our calculated results.

4. Conclusion

In summary, a complete theoretical analysis of the electronic, magnetic and elastic properties of ε-Fe_3X (X=B/C/N) has been presented by means of the first-principles calculations. The calculated equilibrium structural parameters of Fe_3C and Fe_3N are in agreement with the experimental results. Using the same calculating method the crystal structure of the ε-Fe_3B is predicted. In the view of formation energy, the phase stability grows up from ε-Fe_3B, θ-Fe_3N, ε-Fe_3C, θ-Fe_3C, θ-Fe_3B to ε-Fe_3N. The formation energies of ε-Fe_3N (-0.255 eV/f.u.) and θ-Fe_3B (-0.08 eV/f.u.) are negative, which indicates that the formation of ε-Fe_3N and θ-Fe_3B are easier than other phases in the steels or Fe-N/B alloys. From the calculated results, it is confirmed that the bonds of ε-Fe_3X (X=B/C/N) are the complex mixtures of metallic, covalent and ionic characters. The magnetic moments of Fe are 2.17, 2.23 and 2.25 μ_B in ε-Fe_3B, ε-Fe_3C and ε-Fe_3N, respectively. The Ms of B/C/N are $-0.39/-0.26/-0.08$ μ_B. The average magnetic moments of the ε-Fe_3B, ε-Fe_3C and ε-Fe_3N are 1.53, 1.61 and 1.66 μ_B/atom, respectively. The bulk modulus (B), shear modulus (G), Young's modulus (E), and Poisson's ratio (v) of ε-Fe_3B, ε-Fe_3C and ε-Fe_3N are calculated. The Debye temperatures (θ_D) of ε-Fe_3X (X=B/C/N) are predicted as 427, 565 and 555 K, respectively.

Acknowledgments

This research was supported by the Natural Science Foundation of China (no.51101137 and no.51171161) and the Natural Science Foundation of Hebei Province of China (no.E2011203055 and E2011203131).

References

[1] J.W. Simmons, Materials Science and Engineering A 207 (1996) 159.
[2] K.H. Lo, C.H Shek, J.K.L Lai, Materials Science and EngineeringR 65 (2009) 39.
[3] J.W. Christian., The theory of Transformations in metals and Alloys, Pergamon Press, Amsterdam, 2002.
[4] F.H. Sanchez, M.B Fernandez van Reap, J.I Budnick, Physical Review B 46 (1992) 13881.
[5] Hanan Shechter Moshe Ron, S Niedzwiedz, Journal of Applied Physics 39 (1968) 265.
[6] K.H. Jack, Journal of the Iron and Steel Institute, London 169 (1951) 26.
[7] C.M. Fang, M.A. van Huis, H.W. Zandbergen, Scripta Materialia 63 (2010) 418.
[8] C.M. Fang, M.A. van Huis, H.W. Zandbergen, Scripta Materialia 64 (2011) 296.
[9] Jae Hoon Jang, In Gee Kim, H.K.D.H. Bhadeshia, Scripta Materialia 63 (2010) 121.
[10] Dieter Rainer Niewa, Aron Rau, Katrin Wosylus, Michael Hanfland Meier, et al., Chemistry of Materials : A Publication of the American Chemical Society 21 (2009) 392.
[11] T. Liapina, A. Leineweber, E.J. Mittemeijer, W. Kockelmann, Acta Materialia 52 (2004) 173.
[12] S. Shang, A.J. Bottger, M.P. Steenvoorden, M.W.J. Craje., Acta Materialia 54 (2006) 2407.
[13] Fashen Li. Yong Kong, Physical Review B 56 (1997) 3153.
[14] N.I. Medvedeva, I.R. Shein, O. Yu.Gutina, A.L. Ivanovskii, Physics of the Solid State 49 (2007) 2298.
[15] Z.Q. Lv, F.C. Zhang, S.H. Sun, Z.H. Wang, P. Jiang, W.H. Zhang, W.T. Fu, Computational Materials Science 44 (2008) 690.
[16] Z.Q. Lv, W.T. Fu, S.H. Sun, Z.H. Wang, W. Fan, M.G. Qv, Solid State Sciences 12 (2010) 404.
[17] Z.Q. Lv, W.T. Fu, S.H. Sun, et al., Journal of Magnetism and Magnetic Materials 323 (2011) 915–919.
[18] C.X. Wang, Z.Q. Lv, W.T. Fu, Y. Li, S.H. Sun, B. Wang, Solid State Sciences 13 (2011) 1658–1663.
[19] H.L.J. Yakel, International Metal Reviews 30 (1985) 7.
[20] H. Jacobs, D. Rechenbach, U. Zachwieja, Journal of Alloys and Compounds 227 (1995) 10.
[21] Z.J. Wu, E.J. Zhao, H.P. Xiang, X.F. Hao, X.J. Liu, J. Meng, Physical Review B 76 (2007) 054115.
[22] W. Kohn, L.J. Sham, Physical Review A 140 (1965) 1133.
[23] P. Hohenberg, W. Kohn, Physical Review B 136 (1964) 384.
[24] M.D. Segall, P.J.D. Lindan, M.J. Probert, C.J. Pichard, P.J. Hasnip, S.J. Clark, M.C. Payne, Journal of Physics: Condensed Matter 14 (2002) 2717.
[25] J.A. White, D.M. Bird, Physical Review B 50 (1994) 4954.
[26] J.P. Perdew, K. Burke, M. Ernzerhof, Physical Review Letters 77 (1996) 3865.
[27] D. Vanderbilt, Physical Review B 41 (1990) 7892.
[28] H. Jmonkhorst, J.D. Pack, Physical Review B 13 (1976) 5188.
[29] S. Tian, Materials Physical Properties, Beijing University of Aeronautics and Astronautics Press, Beijing, 2004.
[30] L. Fast, J.M. Wills, B. Johansson, O. Eriksson, Physical Review B 51 (1995) 17431.
[31] F.D. Murnaghan, Proceedings of the National Academy of Sciences of the United States of America 30 (1944) 244.
[32] M.J. Mehl, B.M. Barry, D.A. Papaconstantopoulos, Intermetallic compounds: principle and practice, in: J.H. Westbrook, R.L. Fleischeir (Eds.), Principles, I, Wiley, London, 1995, p. 195. Chapter 9.
[33] A. Reuss, Zeitschrift für Angewandte Mathematik und Mechanik 8 (1929) 55.
[34] W. Voigt, Lehrbush der Kristallphysik, Taubner, Leipzig, 1928.
[35] R. Hill, Proceedings of the Physical Society of London A 65 (1952) 349.
[36] E. Schreiber, O.L. Anderson, N. Soga, Elastic Constants and their Measurements, McGraw-Hill, New York, 1973.
[37] S.Q. Wu, Z.F. Hou, Z.Z. Zhu, Solid State Sciences 11 (2008) 251.
[38] V. Kanchana, G. Vaitheeswaran, A. Savane, A. Delin, Journal of Physics: Condensed Matter 18 (2006) 9615.